JOURNAL OF CATALYSIS 103, 426–435 (1987)

Diffusion and Adsorption of Titanium Oxide on Platinum as Related to Strong Metal–Support Interactions

R. VANSELOW AND M. MUNDSCHAU

Department of Chemistry and Laboratory for Surface Studies, University of Wisconsin, Milwaukee, Wisconsin 53201

Received May 14, 1986; revised September 23, 1986

Investigations by field emission microscopy show that two distinguishable Ti oxide layers are formed on rounded Pt crystallites by diffusion from an oxygen-deficient TiO_2 vapor deposit. Layer I, appearing at 700 K, covers all high Miller index areas, {110}, and the vicinal areas of {100}. Layer II is formed at 800 K. In contrast to Layer I, it exhibits a layer boundary. Layer II covers all crystallographic areas except {111}. When it breaks up upon heating above 800 K, numerous high work function islands ($\sim 2 \times 10^{10}$ cm^{-2}) are formed in the high Miller index areas. Because of the large work function difference between these islands and their surroundings, very strong electrostatic fields (patch fields) are created. The islands grow at elevated temperatures and disappear at about 1100 K. Above this temperature, Ti oxide is adsorbed only in the vicinal areas of {111} (1100 to 1200 K) and on {100} (1200 to 1240 K). The possible influence of the patch fields on chemical surface reactions is discussed.

1. INTRODUCTION

Strong metal–support interactions (SMSI) affect adsorption (*1, 2*) and reactivity (*3–6*). They can cause changes in the morphology of metal catalyst crystals (*7, 8*). A variety of models have been developed to explain these phenomena (*9–15*). In the case of larger metal crystals, increasing evidence points to the diffusion and adsorption of support material onto the metal surface (*16–28*). (SMSI has been observed on metal crystals larger than 50 Å (*16, 29, 30*).) It could even be demonstrated that SMSI-like effects can be obtained when support material is directly deposited onto a Group VIII metal (*23, 24, 31*).

One of the catalytic systems that has been studied extensively in connection with SMSI is Pt/TiO_2. Platinum shows very pronounced SMSI effects; titanium oxides require relatively low reduction temperatures to induce SMSI. There can now be little doubt that SMSI of Pt/TiO_2 is accompanied by a partial reduction of the TiO_2 surface regions (*32, 33*). The active species appears to be a Ti oxide rather than the Ti metal itself (*17, 34*).

Additional information is needed for a more complete interpretation of the effects. A direct observation of the surface diffusion and adsorption behavior of Ti oxide on a rounded Pt crystal, for example, would provide useful data. Since field emission microscopy has been used successfully to study oxide diffusion on metal single crystals(e.g. (*35, 36*)), and since the apex crystal of a field emitter can be used to model larger, rounded catalyst particles, the field emission microscope (FEM) is a suitable instrument for such investigations.

The present paper describes the observation of surface diffusion and adsorption behavior of Ti oxide on Pt single crystals by means of FEM. (For comparative purposes, Ti metal on Pt has also been studied.)

2. EXPERIMENTAL PROCEDURE

A standard, bakeable FEM with a vapor deposition source was used (*37*). The residual gas pressure during the experiments

0021-9517/87 $3.00

was in the lower 10^{-10} Torr to the upper 10^{-11} Torr range. Field emitters were prepared from 99.999% pure Pt wires (0.127 mm diameter; Materials Research Corp.) by electrolytic etching with alternating current in a 20 wt% aqueous KCN solution.

A tungsten heating coil served as the evaporator for TiO_2. The tungsten coil was cleaned by electrolytic etching and by subsequent heating under ultrahigh vacuum (UHV). After the cleaning, the coil was loaded with an aqueous TiO_2 paste (TiO_2; Polyresearch Corp., 99.95% pure, Lot T-733). Before mounting the evaporator in a lateral position next to the emitter apex, the TiO_2 was sintered under UHV.

Ti metal was evaporated from a Ti coil which had been electrolytically etched and degassed under UHV.

After the bake-out of the FEM, the emitter electrodes and the emitter assembly were degassed. The emitter was heated and repeatedly flashed at high temperatures. It was finally checked for indications of impurity segregation (*37*) which might have interfered with the investigations on Ti oxide. Emitters with recognizable impurity segregation were rejected. After cleanliness of the emitter surface had been established, the evaporator coil was annealed by resistive heating and Ti oxide was deposited onto the emitter. The latter was at room temperature during the deposition. In the initial trials, the deposit was immediately removed from the tip by heating to eliminate atmospheric impurities which had been adsorbed during evaporator preparation and bake-out.

After the conclusion of these preparatory procedures, a small amount of Ti oxide ($\Theta \approx 3$; the coverage was estimated by using calculated TiO_2 vapor pressure values (*38*)) was deposited onto the clean Pt. Because of the lateral position of the evaporator, only a fraction of the apex crystal, that facing the evaporator, was coated. After the deposition, the emitter was heated stepwise for 30 s at increasing temperatures. (During oxide deposition, as well as during all heat treatments, the electrical imaging potential was zero.) After each heating step, the emitter was rapidly quenched to room temperature and a photograph was taken of the respective surface condition. When, finally, temperatures were reached at which the clean surface reappeared, the Pt surface was thoroughly cleaned by flashing, the amount of Ti oxide deposited was slightly increased, and the heating sequence was repeated.

Similar procedures were followed in the case of Ti metal deposition.

An important question concerns the stoichiometry of the Ti oxide deposit. From the point of view of thermodynamics, the system of Ti oxides is a complex one (*39*). However, according to more recent investigations, the following facts, pertinent to our investigations, appear to be established.

The congruently vaporizing phase is $Ti_3O_{5(s)}$ (*40*). The chemical reaction accounting for the congruent vaporization is (*41, 42*).

$$Ti_3O_{5(s)} = TiO_{(g)} + 2TiO_{2(g)}. \qquad (1)$$

Both TiO and TiO_2 have been detected over vaporizing TiO_2 by mass spectrometry (*43*). The partial pressure of oxygen during the evaporation at 2270 K is in the 10^{-10} Torr range (*44*).

On the basis of these findings, it appears reasonable to assume that the Ti oxide deposits used in our investigations are oxygen deficient with respect to TiO_2 and that they are suitable to simulate TiO_2 after partial reduction with hydrogen.

3. EXPERIMENTAL RESULTS

3.1. Titanium Deposition

Titanium metal deposited onto clean Pt—with the substrate at room temperature—formed coherent layers at modest deposition rates. The electron emission from the deposit layer was so strong that details in the uncovered Pt regions could no longer be recognized. Within the deposit layer, the appearance of the Pt equilibrium planes,

{111} and {100}, remained unchanged (compare Fig. 1a to 1b). Upon heating, no special adsorption or surface reaction patterns could be observed. Above 950 K the pattern of the clean Pt surface (Fig. 1a) reappeared and the emission voltage returned to that of the flashed surface (Fig. 1a).

3.2. *Titanium Oxide Deposition*

After the deposition of Ti oxide ($\Theta \approx 3$) onto a clean Pt surface held at room temperature (the clean surface is depicted in Fig. 2a), the emission dropped drastically over the deposit area (Fig. 2b; arrows indicate deposit boundary). In most cases, the deposit covered only about one-fourth of the imaged surface area. The emission from the deposit-free Pt surface area decreased only slightly.

After heating to 700 K, the first indications of surface migration from the deposit into the originally uncovered area (formation of Layer I) appeared: (i) The emission from the originally uncovered high Miller index areas increased slightly, indicating the presence of an adsorbate. (ii) Adsorption could also be observed in the {110} area and the vicinal areas of {100} ({111} areas remained unchanged). In addition, the boundary of the deposit became more pronounced (Fig. 2c; arrows mark deposit boundary).

After heating to 800 K, an adsorbate layer boundary became visible (Fig. 2d; arrows indicate layer boundary). This newly formed layer, which covered all crystallographic areas except {111}, will be called Layer II. At this point, the difference in emission between Layer I and Layer II was not very strong. The layer boundary became more pronounced after heating at 830 K. At this temperature, very small islands of reduced emission (or increased work function; in the following, these islands will be called "high work function islands") started to form within Layer II. Some of them grew beyond the layer boundary (Fig. 2e). At this stage, the deposit boundary had receded and had moved out of the image region. After heating at 890 K, the layer boundary became most pronounced and the number of high work function islands reached a maximum with an island density of about 2×10^{10} per cm^2 (Fig. 2f).

With increasing temperature (940 to 1070 K), the high work function islands grew in size, while their number decreased (Figs. 2f–h). At the early growth stage, the emission difference between high work function islands and their surroundings was not as distinct as at the advanced stages (Figs. 2f–h). From a certain size on, the islands grew but their emission remained constant at an extremely low value (Figs. 2h–k). At 940 K, the layer boundary had disappeared. However, its former position remained marked by a string of high work function islands (Fig. 2g). With the disappearance of the layer boundary, the (010) plane became adsorbate free and the emission from all high Miller index areas, if not covered by high work function islands, became very even.

During their growth (940 to 1070 K; Figs. 2g–k), the high work function islands constantly changed their shape. In one case, coalescence of three small islands into a larger one was observed. At 1070 K, the island density had dropped to about 1×10^9 per cm^2. All high work function islands disappeared upon heating at 1100 K (Fig. 2l).

Except for the strongly emitting vicinal areas of {111} ({111}-rings), at 1100 K the Pt surface (Fig. 2l) very much resembled a clean surface. (Fragments of {111}-rings had appeared already briefly at about 950 K; see Figs. 2g and h.) This pattern remained fairly unchanged up to 1200 K. At about 1200 K, very small, strongly emitting clusters could be observed on the central (010) plane (Fig. 2m). At about 1230 K, the {111}-rings started to disappear and a strongly emitting, face-specific layer grew on the (010) plane ({100}-layer) (Fig. 2n). This {100}-layer disappeared at 1240 K. Above this temperature, surface features attributable to adsorption could no longer be observed.

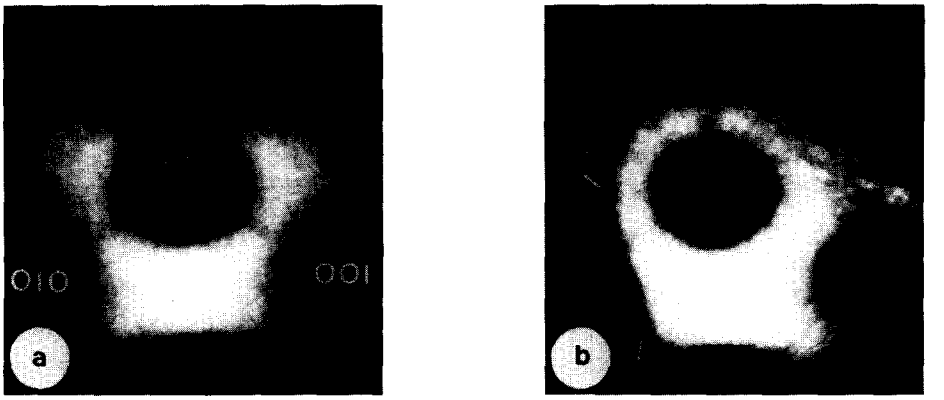

FIG. 1. Field emission micrographs: Ti metal deposition on {111}-centered Pt single crystal. (a) After flashing emitter to 1700 K and subsequent rapid quenching to room temperature (Miller indices mark equilibrium planes). (b) After initial deposition of Ti. During deposition, emitter was at room temperature and the imaging potential was zero. Deposition occurred from the upper right corner. Arrows mark deposit boundary. Deposit appears brighter than uncovered Pt areas.

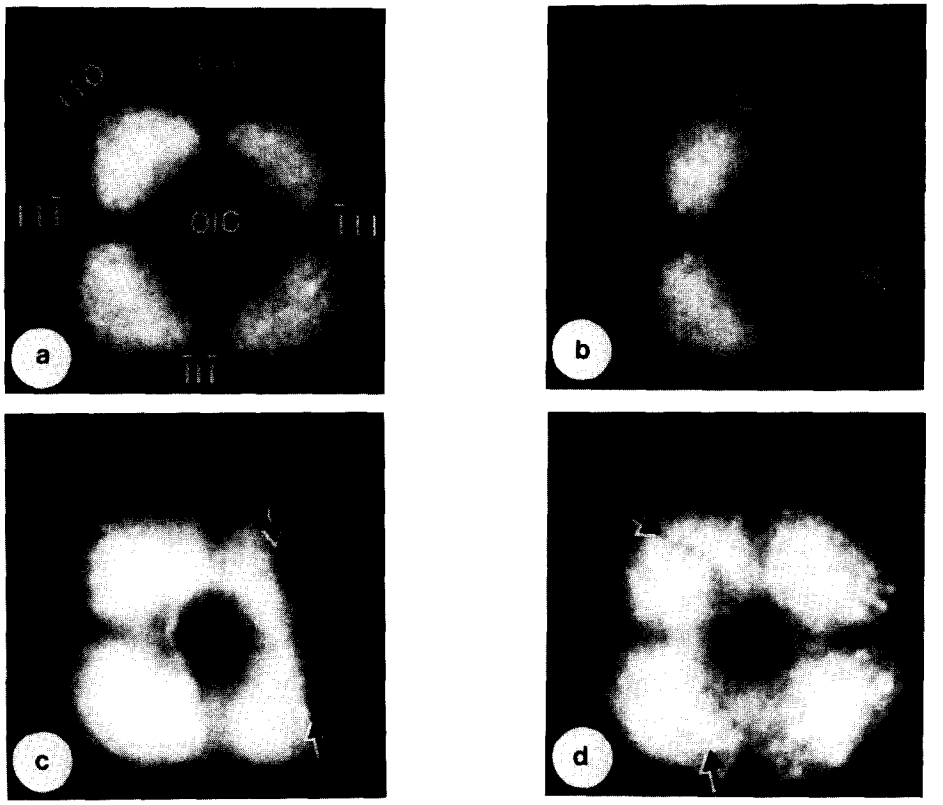

FIG. 2. Field emission micrographs: Ti oxide on Pt. After deposition, the emitter was heated stepwise for 30 s at increasing temperatures. The imaging potential was zero during all heat treatments. For each micrograph, the respective annealing temperature is indicated. (a) After flashing emitter to 1700 K and subsequent rapid quenching to room temperature. Emitter crystal is {010}-centered. Miller indices mark {111}, (010), and position of (110). (b) After initial deposition of Ti oxide. During deposition emitter was at room temperature and the imaging potential was zero. Deposition occurred from the right-hand side. Arrows mark deposit boundary. (c) 700 K. (d) 800 K. (e) 830 K. (f) 890 K. (g) 940 K. (h) 960 K. (i) 1020 K. (j) 1035 K. (k) 1070 K. (l) 1095 K. (m) 1205 K. (n) 1225 K. After heating to higher temperatures, micrograph (a) reappeared.

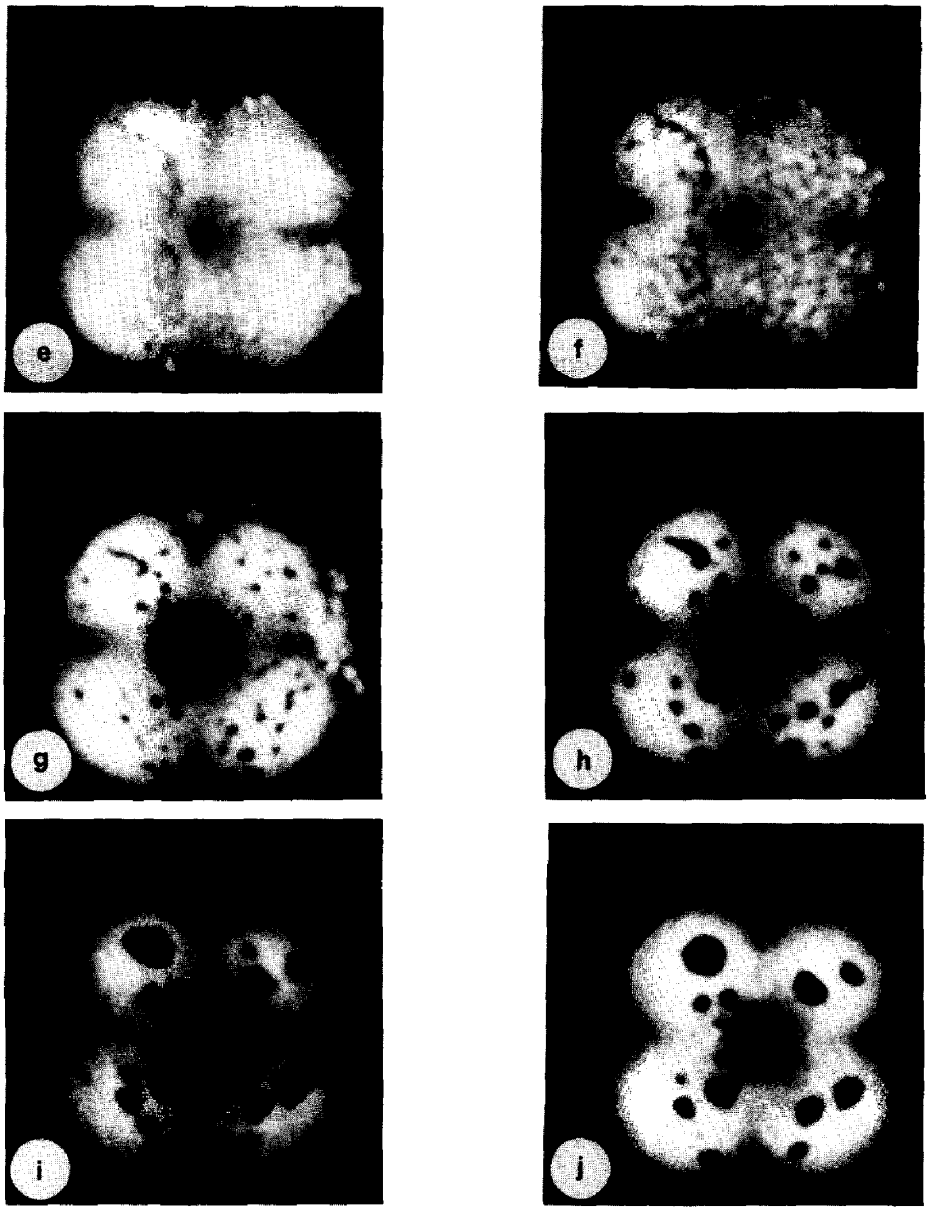

FIG. 2—*Continued.*

The images returned to that of the clean surface (Fig. 2a).

When the initial Ti oxide deposit was doubled ($\Theta \approx 6$), large bright clusters in the vicinity of {111}, as well as {111}-rings, appeared already between 840 and 950 K. A fourfold increase in the initial deposit ($\Theta \approx 12$) resulted in the formation of very large, strongly emitting clusters. Emitters with such heavy coverages were in most cases destroyed during imaging.

4. DISCUSSION AND CONCLUSIONS

4.1. Titanium on Platinum

Titanium metal deposited onto Pt shows Frank–van der Merwe growth. Since the average work function of Ti (ϕ(Ti) = 3.95

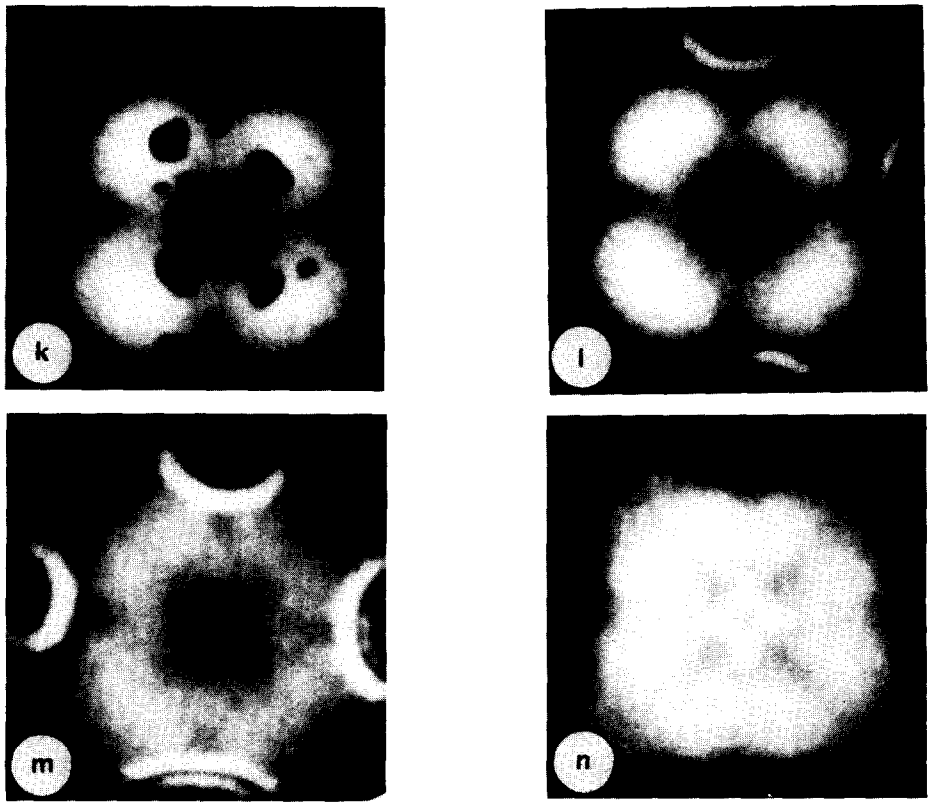

FIG. 2—*Continued.*

eV (*45*)) is considerably smaller than that of Pt (ϕ(Pt) = 5.32 eV (*45*)), the electron emission originates almost completely from the deposit layer. The observation that Ti of the overlayer dissolved into the Pt bulk at moderate temperatures ($T < 950$ K) is consistent with the fact that Ti readily alloys with Pt. After the dissolution, Ti does not reappear on the surface upon heating at any temperature. This is in agreement with the prediction that Ti in Pt–Ti alloys will not segregate to the surface (*46*, *47*).

4.2. Titanium Oxide on Platinum

After the deposition of Ti oxide, a slight increase in the work function of the deposit-free Pt area was observed. This might indicate the adsorption of a fraction of a monolayer of oxygen. As pointed out earlier, oxygen has been observed during the evaporation of TiO_2 (*44*).

First indications of surface migration from the deposit layer into the originally deposit-free surface area can be recognized after heating for 30 s at 700 K. (It should be pointed out that prolonged annealing times, as applied, for example, during the preparation of a catalyst, will shift the features observed here to lower temperatures.) The temperature of 700 K lies at about one-third of the melting point of those Ti oxides which have to be considered in the present investigation. The fraction of roughly one-third of the absolute melting point of the deposit is typical for oxides and has also been observed, for example, for Al oxide on Ir (*48*), Re (*36*), and W (*49*). Since the emission patterns obtained after the migration of Ti oxide do not resemble those recorded after Ti deposition and annealing, it is assumed that the migrating species are Ti oxide(s) (TiO and/or TiO_2). The migration

at 700 K occurs without formation of a diffusion layer boundary. The resulting adsorbate layer covers the high Miller index areas and causes a slight work function decrease. The layer cannot be observed on {111} or {100}.

Between 700 K and 800 K, a second, coherent oxide layer spreads from the deposit layer. It appears that the molecules migrate over the already existing Layer II surface and that they are incorporated into the layer when they move over its boundary edge. This "carpet roll mechanism" is responsible for the formation of the pronounced layer boundary. Except for {111}, Layer II covers all surface areas of the Pt crystal.

Upon heating above 800 K, Layer II becomes unstable and rearrangements occur. The formation of high work function islands can be observed. It seems that the layer edge promotes the island nucleation, because at 800–830 K, high work function islands appear preferentially along and in the closer vicinity of the layer boundary. At 830 K, their formation can be observed in all high Miller index areas throughout Layer II. At 940 K, Layer II is completely broken up. Ostwald ripening and constant shape changes of the high work function islands indicate a high surface mobility in this temperature range.

High work function islands (on top of a preadsorbed low work function layer) are formed by various metal oxides (*35, 36, 50, 51*). The most thoroughly investigated system is that of Al oxide (*35, 36, 49, 53*). However, except for the system described here (Ti oxide/Pt), high work function island formation is normally restricted to specific crystallographic directions (face specific island growth). In the case of Al oxide/W, for example, a large high work function island occurs only on {100}. Müller was the first to suggest that the surface of high work function islands is formed by oxygen (*50*). This hypotheses was supported by A. Many (*52*). Negatively charged surface oxygen would indeed lead to a drastic work function increase. Pankow (*53*) estimated a work function of about 7 eV over Al oxide islands on W{100}. Work function measurements on this system indicate a work function difference between the preadsorbed low work function layer and high work function island of $\Delta\phi \approx 3$ eV.

In the case of Ti oxide/Pt, the statistically distributed high work function islands grow from a few angstroms to about 1000 Å in diameter. Because of the large work function difference, the formation of high work function islands will be accompanied by the creation of strong electrostatic fields (so called patch fields (*54, 55*)).

Such patch fields are not limited to field emitters and their formation and existence does not require the application of any external electric field. They can occur on any surface if it contains very small islands with work functions sufficiently different from their surroundings. The work function of the islands can be higher or lower than that of the surroundings. Patch fields may even occur on a clean metal single crystal, if the latter is rounded and if its equilibrium planes appear as flat areas (*55*). For Pt, for example, the work function difference between {111} and the surrounding curved high Miller index areas is about 0.8 eV. For small enough metal crystals, strong patch fields will occur also in this case. Extremely strong patch fields should be obtained when small alkali metal islands are formed, for example, on the above-mentioned high work function oxide layers. (Such a combination (K/Al_2O_3) is used, for example, in doubly promoted iron (ammonia) catalysts (e.g. (*56*)).)

The size of a patch field, F_p, at the surface is determined by the work function difference, $\Delta\phi$, between a patch (island) and its surroundings and by the patch radius, R_p (e.g. (*55*)).

$$F_p = \frac{\Delta\phi}{R_p} \quad \text{(V/cm)} \tag{2}$$

$$\Delta\phi = \phi_{patch} - \phi_{surr.} \quad \text{(V)}. \tag{3}$$

Another relation, leading to patch fields larger than those described by Eq. (2) by a factor of about 8, has been derived by Politzer and Feuchtwang (*57*). Using Eq. (2) and the above quoted $\Delta\phi$ of 3 eV, one obtains for high work function islands with radii of 5, 30, 50, 100, and 500 Å, patch fields of 6×10^7, 1×10^7, 6×10^6, 3×10^6, and 6×10^5 V/cm, respectively.

Such patch fields could have strong effects on the thermodynamics as well as the kinetics of surface reactions. The dependence of the rate constant, k, on the electric field, F_e, is given by

$$\left(\frac{d(\ln k)}{dF_e}\right)_{p,T} = \frac{\Delta\mathfrak{M}^{\ddagger}}{k_B T} \quad (4)$$

$$\Delta\mathfrak{M}^{\ddagger} = (\mu^{\ddagger} - \Sigma\mu_r) F_e + \tfrac{1}{2}(\alpha^{\ddagger} - \Sigma\alpha_r) F_e^2; \quad (5)$$

$k_B \equiv$ Boltzmann constant;
$\mu^{\ddagger}, \alpha^{\ddagger} \equiv$ dipole moment and polarizability of the activated complex, respectively; and
$\mu_r, \alpha_r \equiv$ dipole moment and polarizability of the reactant molecules, respectively.

The corresponding thermodynamic (van't Hoff-type) equation has been discussed by Block (*58*), who also could show that for the reaction

$$2\mathrm{HCOOH} \rightleftarrows (\mathrm{HCOOH})_2$$

the equilibrium constant, K, indeed shows a strong field strength dependence (*59*). Calculations were carried out for a field strength range of about 1×10^6–1×10^7 V/cm.

According to Eq. (4), small high work function islands, if formed by support material (Ti oxide) diffusion onto Pt catalyst particles and if stable under catalytic working conditions, should accelerate all those reactions in which $\Delta\mathfrak{M}^{\ddagger}$ is positive and retard the ones with negative $\Delta\mathfrak{M}^{\ddagger}$. There is some similarity between this patch effect on solid surfaces and the solvent effect in the liquid phase. In the latter, according to Glasstone's interpretation of Soper's rule (*60*), reactions with a positive $\Delta\mathfrak{M}$ are accelerated by a polar solvent (while those with negative $\Delta\mathfrak{M}$ are retarded). In the case of the patch effect, the term "solvent polarity" has to be replaced by the term "patch field."

Since Ti oxide, after diffusing onto Pt, also changes the catalyst's adsorption properties, unfortunately, an analysis of SMSI effects with regard to the possible influence of patch fields is not straightforward.

After all high work function islands have been desorbed between 1070 and 1100 K, the Pt surface looks relatively adsorbate free except for the vicinal areas of {111}. Whether or not oxide precipitates in these areas, and if so, when, depends on the supersaturation. If the Ti oxide deposition is increased, the precipitation occurs at lower temperatures. For example, when the deposition shown in Fig. 2b was doubled, precipitation already occurred at 840 K. This preferential precipitation in the vicinal area of {111} (the step edges of the vicinal area lower the activation energy for nucleation) may indicate a favorable epitaxial fit between oxide and Pt{111}.

All oxides to be considered in these investigations (TiO_2 (rutile structure), Ti_2O_3 (corundum structure), Ti_nO_{2n-1} (n = 3–10; slabs of rutile), and TiO (high temperature, NaCl structure)) have closely packed oxygen net planes. If one assumes that oxygen makes contact at the interface, the misfit (Ti oxide/Pt{111}) turns out to be around +7.6%. Only rutile gives a smaller value because the oxygen net planes are slightly warped. Considering epitaxial mismatch only, Pt{111} should be preferred over other planes. The identical misfit for the various oxides makes it impossible to decide which of the oxides precipitates in the vicinal area of {111}. The above mentioned misfit of +7.6% is relatively small and may explain the precipitate stability. The {111} precipitate can be observed up to 1230 K. At this temperature it coexists briefly with an oxide layer on {100}. Since the rutile basal

plane gives a misfit of only 6.8% Pt{100}, the {100} oxide layer may have a related structure.

At 1240 K all oxide could be removed by heating.

5. SUMMARY

Surface diffusion and adsorption of Ti oxide on Pt was studied by means of FEM to obtain information which might be useful in the interpretation of SMSI effects. Oxygen-deficient TiO_2 deposits were formed in the lateral regions of hemispherical apex crystals of Pt field emitters.

Surface migration from the deposit into the deposit-free Pt area could first be observed after heating at 700 K. The initial adsorbate layer (Layer I) covered all high Miller index areas, {110}, the vicinal areas of {100}, but not {111}.

After heating to 800 K, an additional, coherent oxide layer (Layer II) with a well-developed layer boundary was formed. With the exception of {111}, all other crystallographic areas were covered by Layer II. Both layers cause a slight work function decrease. Upon heating above 800 K, Layer II broke up and numerous high work function islands (island density about 2×10^{10} per cm^2) were formed in the high Miller areas of Pt. The islands showed a random distribution. Because of the large work function difference between the islands and their surroundings ($\Delta\phi \approx 3$ eV), and because of the small size of the islands, very high electrostatic fields (patch fields) are created.

Between 940 and 1070 K, the number of high work function islands decreased (lowest island density about 1×10^9 per cm^2), while their individual size increased. Continuous shape changes of the islands indicate a high surface mobility of the oxide molecules in this temperature range. The high work function islands disappeared at 1100 K.

Above this temperature, titanium oxide was adsorbed in the vicinal area of {111} (1100 to 1200 K) and on {100} (1200 to 1240 K). Above 1240 K the Pt surface appeared adsorbate free.

Studies of Ti adsorption on Pt did not give any indications that the free Ti metal is involved in the formation of the above-described diffusion and adsorption features.

According to the above findings, Ti oxide can affect the catalytic activity of Pt in at least two ways (if the features described here are stable also under catalytic working conditions):

(i) By layer- and/or face-specific precipitate formation, Ti oxide influences the adsorption and diffusion properties of the covered areas.

(ii) By formation of high work function islands, Ti oxide can influence reaction rates through the creation of strong electric patch fields. For example, reactions in which the dipole moment of the activated molecule is larger than the sum of the dipole moments of the reactants will be accelerated.

REFERENCES

1. Tauster, S. J., Fung, S. C., and Garten, R. L., *J. Amer. Chem. Soc.* **100,** 170 (1978).
2. Tauster, S. J., and Fung, S. C., *J. Catal.* **55,** 29 (1978).
3. Vannice, M. A., and Garten, R. L., *J. Catal.* **56,** 236 (1979).
4. Vannice, M. A., and Garten, R. L., U.S. Patent 4,042,614 (1977).
5. Vannice, M. A., and Garten, R. L., U.S. Patent 4,042,615 (1977).
6. Ko, E. I., and Garten, R. L., *J. Catal.* **68,** 233 (1981).
7. Baker, R. T. K., Prestridge, E. B., and Garten, R. L., *J. Catal.* **56,** 390 (1979).
8. Baker, R. T. K., Prestridge, E. G., and Garten, R. L., *J. Catal.* **59,** 293 (1979).
9. Menon, P. G., and Froment, G. F., *Appl. Catal.* **1,** 31 (1981).
10. Otter, G. J., and Dautzenberg, F. M., *J. Catal.* **53,** 116 (1978).
11. Cairns, J. A., Baglin, J. E. E., Coark, G. J., and Ziegler, J. F., *J. Catal.* **83,** 301 (1983).
12. Horsley, J. A., *J. Amer. Chem. Soc.* **101,** 2870 (1979).
13. Chen, B. H., and White, J. M., *J. Phys. Chem.* **86,** 3534 (1982).
14. Greiner, G., and Menzel, D., *J. Catal.* **77,** 382 (1982).

15. Kao, C. C., Tsai, S. C., Bahl, M. K., and Chung, Y. W., *Surf. Sci.* **95,** 1 (1980).
16. Santos, J., Phillips, J., and Dumesic, J. A., *J. Catal.* **81,** 147 (1983).
17. Resasco, D. E., and Haller, G. L., *J. Catal.* **82,** 279 (1983).
18. Mériaudeau, P., Dutel, J. F., Dufaux, M., and Naccache, C., *Stud. Surf. Sci. Catal.* **11,** 95 (1982).
19. Jiang, X. Z., Hayden, T. F., and Dumesic, J. A., *J. Catal.* **83,** 168 (1983).
20. Chung, Y.-W., Xiong, G., and Kao, C.-C., *J. Catal.* **85,** 237 (1984).
21. Sadeghi, H. R., and Henrich, V. E., *J. Catal.* **87,** 279 (1984).
22. Simoens, A. J., Baker, R. T. K., Dwyer, D. J., Lund, C. R. F., and Madon, R. J., *J. Catal.* **86,** 359 (1984).
23. Raupp, G. B., and Dumesic, J. A., *J. Phys. Chem.* **88,** 660 (1984).
24. Vannice, M. A., and Sudhaker, C., *J. Phys. Chem.* **88,** 2429 (1984).
25. Takatani, S., and Chung, Y.-W., *J. Catal.* **90,** 75 (1984).
26. Raupp, G. B., and Dumesic, J. A., *J. Catal.* **95,** 587 (1985).
27. Baker, R. T. K., Chludzinski, J. J., and Dumesic, J. A., *J. Catal.* **93,** 312 (1985).
28. Dumesic, J. A., Stevenson, S. A., Sherwood, R. D., and Baker, R. T. K., *J. Catal.* **99,** 79 (1986).
29. Burch, R. and Flambard, A. R., *J. Catal.* **78,** 389 (1982).
30. Jiang, X.-Z., Stevenson, S. A., and Dumesic, J. A., *J. Catal.* **91,** 11 (1985).
31. Kugler, E. L., and Garten, R. L., U.S. Pate. 4,273,724 (1981).
32. Huizinga, T., and Prins, R., *J. Phys. Chem.* **85,** 2156 (1981).
33. Pajonk, G. M., Teichner, S. J., and Germain, J. F., Eds., "Spillover of Adsorbed Species." Elsevier, New York, 1983.
34. Spencer, M. S, *J. Phys. Chem.* **88,** 1046 (1984).
35. Vanselow, R., Ross, J. P., and Gara, M., *J. Cryst. Growth* **23,** 1 (1974).
36. Beach, T., and Vanselow, R., *Appl. Phys.* **4,** 265 (1974).
37. Mundschau, M., and Vanselow, R., *Surf. Sci.* **155,** 121 (1985).
38. Samsonow, G. V., "The Oxide Handbook," IFI/Plenum, New York/Washington/London, 1973.
39. Wahlbeck, P. G., and Gilles, P. W., *J. Chem. Phys.* **46,** 2465 (1967).
40. Gilles, P. W., Carlson, K. D., Franzen, H. F., and Wahlbeck, P. G., *J. Chem. Phys.* **46,** 2461 (1967).
41. Drowart, J., Coppens, P., and Smoes, S., *J. Chem. Phys.* **50,** 1046 (1969).
42. Hampson, P. J., and Gilles, P. W., *J. Chem. Phys.* **55,** 3712 (1971).
43. Berkowitz, J., Chupka, W. A., and Inghram, M. G., *J. Phys. Chem.* **61,** 1569 (1957).
44. Maissel, L. I., and Glang, R., "Handbook of Thin Film Technology," McGraw–Hill, New York, 1970.
45. Fomenko, V. S. "Handbook of Thermionic Properties," Plenum Press, New York, 1966.
46. Spencer, M. S., *Surf. Sci.* **145,** 145 (1984).
47. Spencer, M. S., *Surf. Sci.* **145,** 153 (1984).
48. Pederson, L. R., Dissertation, University of Wisconsin, Milwaukee, 1978.
49. Ross, J. P., and Vanselow, R., *Appl. Phys.* **4,** 161 (1974).
50. Müller, E. W., *Ergebn. Exact. Naturw.* **27,** 290 (1953).
51. Pankow, G., and Drechsler, M., *Z. Phys. Chem. NF* **31,** 288 (1962).
52. Many, A., private communication.
53. Pankow, G., Dissertation, Technische-Universität, Berlin, 1960.
54. Hatsopoulos, G. N., and Gyftopoulos, E. P., "Thermionic Energy Conversion," Vol. II. MIT Press, Cambridge, MA, 1979.
55. Young, R. D., and Clark, H. E., *Phys. Rev. Lett.* **17,** 351 (1966).
56. Bowker, M., Parker, I. B., and Waugh, K. C., *Appl. Catal.* **14,** 101 (1985).
57. Politzer, J., and Feuchtwang, T. E., *Surf. Sci.* **19,** 443 (1970).
58. Block, J. H., *in* "Chemistry and Physics of Solid Surfaces" (R. Vanselow and S. Y. Tong, Eds.), Vol. I, CRC Press, Boca Raton, FL, 1976.
59. Block, J. H., and Moentack, P. L., *Z. Naturforsch. Teil A* **22,** 711 (1967).
60. Glasstone, S., "Physical Chemistry," McMillan & Co., London, 1966.